NONLINEAR ACOUSTIC BEAM PROPAGATION MODELING IN DISSIPATIVE MEDIA

Jahan Tavakkoli
Department of Physics, Ryerson University, 350 Victoria Street, Toronto, Ontario, M5B 2K3, Canada
jtavakkoli@ryerson.ca

Shahram Mashouf
Department of Medical Biophysics, University of Toronto, Sunnybrook Research Institute
2075 Bayview Ave., Toronto, ON M4N 3M5, Canada

ABSTRACT

Accurate simulation of an intensive ultrasound beam requires taking nonlinear propagation effects into account. A notable example in the field of biomedical ultrasound where the effect of nonlinearity may play a significant role is the high intensity focused ultrasound (HIFU) as a non-invasive energy-based treatment modality. In this work, a 3D numerical model to simulate nonlinear propagation of continuous wave ultrasound beams in dissipative homogeneous tissue-like media is presented. The model implements a second-order operator splitting method in which the effects of diffraction, nonlinearity and attenuation are propagated over incremental steps. The model makes use of an arbitrary 3D source geometry definition method and a non axi-symmetric propagation scheme, which leads to a 3D solution to the resulting nonlinear ultrasound field. This work builds on methods developed by Tavakkoli *et al.* (1998) and Zemp *et al.* (2003) and offers an efficient way to calculate nonlinear field of continuous wave ultrasound sources. The proposed model is a particularly useful computational tool in carrying out simulations of high intensity focused ultrasound beams in soft tissue where the effects of nonlinearity, diffraction, and attenuation are important. The model was validated through comparisons with other established linear and nonlinear numerical models as well as published experimental data.

RÉSUMÉ

La simulation précise d'un faisceau d'ultrasons intensive nécessite de prendre des effets de propagation non-linéaire en compte. Un exemple notable dans le domaine d'ultrasons biomédicale où l'effet de la non-linéarité peut jouer un rôle important est des ultrasons focalisés de haute intensité (HIFU) comme un modalité de traitement fondées sur l'énergie non-invasive. Dans ce travail, un modèle numérique 3D pour simuler la propagation non-linéaire des ultrasons à ondes continues dans un milieu dissipatif et homogène similaire au tissue est présenté. Le modèle met en œuvre une méthode de deuxième ordre d'opérateur dans lequel les effets de diffraction, la non-linéarité et de l'atténuation sont propagées de façon additive. Le modèle utilise une méthode arbitraire de définition de source géométrie 3D et un régime de propagation non-axisymétriques, ce qui conduit à une solution 3D au domaine d'ultrasons non-linéaire qui en résulte. Ce travail s'appuie sur des méthodes développées par Tavakkoli *et al.* (1998) et Zemp *et al.* (2003) qui offre un moyen efficace de calculer le champ non-linéaire des ondes ultrasons continue. Le modèle proposé est un outil particulièrement utile dans l'exercice des simulations numérique des faisceaux ultrasonores focalisés de haute intensité dans les tissus où les effets de la non-linéarité, de diffraction et d'atténuation sont importantes. Le modèle a été validé par des comparaisons avec d'autres établis linéaires et non-linéaires des modèles numériques ainsi que les données expérimentales publiées.

1. Introduction

Propagation of ultrasound is inherently a nonlinear process (Hamilton and Blackstock 1998). Nonlinear effects of ultrasound propagation such as waveform distortion and generation of harmonics can be observed in many biomedical applications of ultrasound (Carstensen and Bacon 1998). Two notable examples where the effects of nonlinear beam propagation play major roles in bioeffects of ultrasound are high intensity focused ultrasound (HIFU) and lithotripsy where intensive and focused ultrasound beams are used for various tissue treatments. Linear equations can be obtained assuming small signal approximations around equilibrium values of pressure and density. As the acoustic pressure and intensity levels are increased within the medium, more deviation from a linear model is expected

(Baker 1998). Analytical solutions to the problem of finite-amplitude propagation of acoustic beam are generally limited to simple geometries under specific simplifying conditions. Several numerical methods have been developed over the years to account for nonlinear propagation of ultrasound beams in various media (Hamilton and Blackstock 1998). These methods are typically focused on finding numerical solutions to appropriate partial differential equations (Ystad and Berntsen 1996, Khokhlova *et al.* 2001, Kamakura *et al.* 2000). One of the equations which has been widely used to describe finite-amplitude propagation of the acoustic beam is the KZK (Khokhlov, Kuznetsov, Zabolotskaya) nonlinear wave equation (Kuznetsov 1971). It accounts for combined effects of diffraction, nonlinearity and absorption and has been validated through comparison with experiments for various source geometries (Baker *et al.* 1988, Averkiou and Hamilton 1995, Baker *et al.* 1995). The KZK equation, however, is only valid in directional beams where paraxial assumption holds true. As a result it fails to be valid close to the source surface, far off the propagation axis, in highly focused sources or when the source dimensions approach one wavelength (Duck 2002). To overcome these limitations, a more general nonlinear propagation model which accounts for full diffraction was proposed (Christopher and Parker 1991, Tavakkoli *et al.* 1998). In this model the propagation of the acoustic field is carried out using a method of fractional-steps. Then, Zemp *et al.* (2003) extended the works of Christopher and Parker and Tavakkoli *et al.* to simulate nonlinear propagation of array transducers in dissipative homogeneous tissue-like media. In this work we extend the work of Zemp *et al.* to general 3D transducer geometries which are used in simulations of high intensity focused ultrasound beams.

2. Materials and Methods

Method of fractional steps

In our model the field is calculated plane by plane in a marching scheme. Consider a partial differential equation in the form of an evolution equation as:

$$\frac{\partial f}{\partial z} = \mathrm{L}_{x,y,t}\{f\} \tag{1}$$

where f is a function of x,y,z,t and $\mathrm{L}_{x,y,t}\{f\}$ is an operator which only acts on x,y,t dimensions. The term $\partial f/\partial z$ on the left side of the equation enables plane by plane calculations of the function f in incremental steps along the z axis provided the values of f is known on an initial plane (e.g. at $z=0$). This method is commonly referred to as method of fractional steps (Ames 1992). The KZK equation can also be written in a form similar to Eq. (1) as shown below (Cobbold 2007, pp. 254):

$$\frac{\partial p}{\partial z} = \frac{c_o}{2}\int_{-\infty}^{\tau}\nabla_{\perp}^2 p d\tau + \frac{1}{2c_o^3\rho_o}\left[\left(\mu_B + \frac{4}{3}\mu\right)\frac{\partial^2 p}{\partial \tau^2} + \beta\frac{\partial p^2}{\partial \tau}\right] \tag{2}$$

The first term in the right hand side of Eq. (2) represents diffraction, the second term accounts for attenuation and the third term appears because of nonlinearity. In our model, however, as will be explained in the next section, the diffraction operator is different from what is used in the KZK equation.

As it was suggested by Tavakkoli *et al.* (1998), the right hand side of Eq. (2) can be divided into three parts and rewritten in a general evolution equation form as below:

$$\frac{\partial p}{\partial z} = \mathrm{L}_D\{p\} + \mathrm{L}_A\{p\} + \mathrm{L}_N\{p\} \tag{3}$$

where $\mathrm{L}_D\{p\} = \frac{c_0}{2}\int_{-\infty}^{\tau}\nabla_{\perp}^2 p\, d\tau$ is the diffraction operator, $\mathrm{L}_A\{p\} = \frac{1}{2c_0^3\rho_0}\left(\mu_B + \frac{4}{3}\mu\right)\frac{\partial^2 p}{\partial \tau^2}$ is the attenuation operator and $\mathrm{L}_N\{p\} = \frac{1}{2c_0^3\rho_0}\left(\beta\frac{\partial p^2}{\partial \tau}\right)$ represents the operator of nonlinearity. Eq. (3) demonstrates how operators of diffraction, nonlinearity and attenuation can be applied independently and then the results are added together. This is referred to as operator splitting method and has been schematically illustrated in Fig. 1(a). In our model, however, we have made use of a second-order operator-splitting method which follows a certain propagation scheme as illustrated in Fig. 1(b). Using the second-order operator splitting method would enable using larger propagation steps while maintaining the same degree of accuracy (Tavakkoli *et al.* 1998).

Diffraction operator

Using the second-order operator splitting method, the first step in propagating the field from the initial plane involves a half step diffractive propagation as shown in Fig. 1(b). The main difference between this method and implementation of the KZK equation lies in the diffraction step. The diffraction term of $\frac{c_0}{2}\int_{-\infty}^{\tau}\nabla_{\perp}^2 p\, d\tau$ in the right hand side of the KZK Eq. (2) is only an approximation based on paraxial assumption. A more general term for diffraction should account for pressure distribution over the entire propagation plane and not only for the transversal Laplacian of pressure at each point. In this method the diffraction term in the KZK equation is replaced by a full diffraction solution. This is achieved by an angular spectrum approach which enables plane to plane diffractive propagation. If two planes are perpendicular to the z axis and Δz is the distance between them, we have (Cobbold 2007 pp.125, Zemp *et al.* 2003):

$$s(x,y,z+\Delta z) = \Im_{2D}^{-1}\left\{\Im_{2D}\{s(x,y,z)\}\times H(k_x,k_y,\Delta z)\right\} \tag{4}$$

where the transfer function $H(k_x,k_y,\Delta z) = e^{j\Delta z\sqrt{k^2-(k_x^2+k_y^2)}}$, $k = 2\pi(nf_o)/c_o$ and n is the harmonic number. The term $s(x,y,z)$ in Eq. (4) could be any field parameter such as pressure, normal particle velocity or velocity potential. In our model, we choose to propagate the normal particle velocity (i.e. $s(x,y,z) = v_z(x,y,z)$), since in our model the nonlinearity and attenuation operator acts on the normal particle velocity as discussed below.

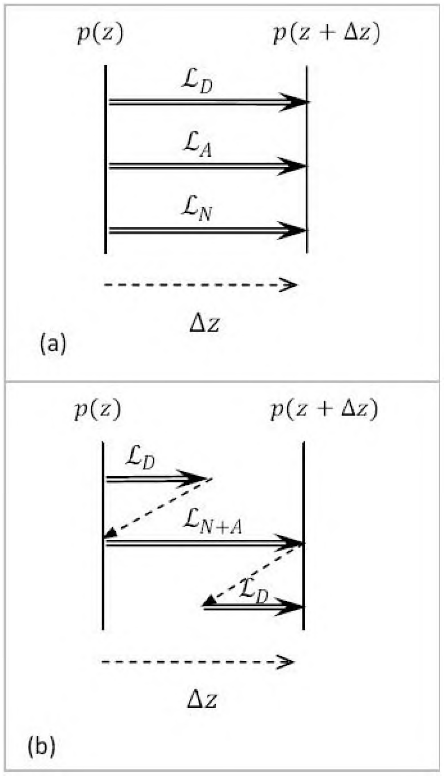

Figure 1. Operator splitting methods. (a) First order, and (b) second order.

Nonlinearity and attenuation operators

After finishing with the diffractive sub-step, the results are converted to the spatial domain and a nonlinearity and attenuation sub-step is subsequently followed as shown in Fig. 1(b). Combined effects of nonlinearity and attenuation are applied in one step using the solution obtained by Harran and Cook (Haran and Cook 1983) for nonlinear propagation of progressive plane waves in lossy media. In this method a finite number of harmonics (N) is captured at each plane and normal particle velocity at $z + \Delta z$ is obtained from the harmonic values of the preceding plane as below:

$$v_n(z+\Delta z) = v_n(z) + j\frac{2\pi\beta f_o}{2c_o^2}\Delta z\left[\sum_{i=1}^{n-1} i v_i v_{n-i} + \sum_{i=n+1}^{N} n v_i v_{n-i}^*\right] - \alpha_o (nf_o)^\eta v_n \Delta z \quad (5)$$

where n is the harmonic number. Eq. (5) has to be repeated N times to calculate all harmonics for each propagation step.

3D source definition

The first step in calculating the nonlinear acoustic field is to propagate the field from the surface of the transducer to a plane close-by which is called the initial plane. The reason behind this is that the method of fractional steps and the angular spectrum technique are both based on plane by plane propagation while the source geometry in general can presume any non-planar shape. The first part of the problem is to introduce a method to fully describe any source geometry and the second part is to introduce a method to capture the field of an arbitrarily shaped transducer. The first part is handled though introduction of an elements matrix and the second part is solved by using the Rayleigh diffraction integral on the surface of the source. To be able to define any source geometry and excitation, the source is broken into an array of small rectangular elements. The elements specifications (location and excitation) are then saved into a 16×N matrix which we refer to as the *Source Elements Matrix*. N is the total number of small rectangular surface elements and 16 is the number of attributes required to fully describe a surface element (Mashouf 2009).

Full diffraction solution

Since our method accounts for full diffraction, it is desirable that the first propagation step would also include full diffraction calculation. Furthermore it is important to have the field calculated on the initial plane as accurate as possible in order to minimize the effect of error propagation due to plane by plane propagation scheme in the method of fractional steps. In light of this, the field on the initial plane is calculated using the Rayleigh diffraction formula which is a surface integral over the entire source area as shown in Fig. 2(a). Alternatively one can use a phase shift method to estimate the field on the initial plane based on the value of the closest surface element by applying phase and amplitude correction factors as shown in Fig. 2(b). This method has been widely used for simulations of a spherically concaved transducer (Averkiou and Hamilton 1995, Christopher and Parker 1991, Filonenko and Khokhlova 2001). Although it is computationally less intensive, this method is an approximate solution and could yield in significant errors for highly focused sources (Mashouf 2009). This can be explained by noting that the field at any point on the initial plane is a sum of contributions of all surface elements and cannot be simply presented by a phase and/or amplitude correction to the corresponding value at the source surface. Once the geometry and excitation of the source are defined, the pressure is calculated at discrete points on the initial plane (e.g. point A in Fig. 2-a) by making use of the Rayleigh diffraction integral over the entire surface of the source as below (Ocheltree and Frizzell 1989):

$$P_A = \frac{j\rho_o c_o}{\lambda}\int_S V_n \frac{e^{-(\alpha+jk)r}}{r} dS \quad (6)$$

where r is the distance between the field point and an infinitesimal surface element, V_n is the normal velocity phasor at the element surface and dS is the area of the infinitesimal surface element.

Since in our model, the source is defined by a set of small rectangular elements, Eq. (6) is realized as below:

$$P_A = j\frac{\rho_o c_o}{\lambda}\sum_{i=1}^{N} V_{ni} \frac{e^{-(\alpha+jk)r_i}}{r_i} \times w \cdot l \quad (7)$$

where N is the total number of surface elements, r_i is the distance between the field point and the center of the ith surface element, and w and l are the width and the length of each surface element respectively.

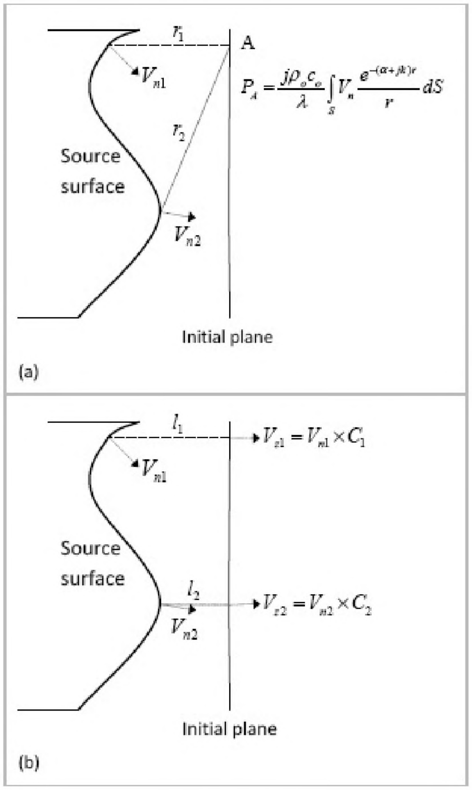

Figure 2. Schematic demonstration of the ultrasound field calculation over an initial plane by (a) implementing the Rayleigh diffraction integral, (b) introducing phase/amplitude correction factors. In method (a) contributions of all surface elements are taken into account while in method (b) only the value of the closest horizontally located element is used to estimate the field by applying a complex correction factor (C_1, C_2).

Field propagation

Field propagation is done in incremental steps following a second-order operator splitting method as described earlier. The first step involves a half step diffractive propagation as illustrated in Fig. 1(b). Each harmonic is propagated separately by applying Eq. (4) as below:

$$\Im_{2D}\{v_z(x,y,z+(\Delta z/2))\} = \Im_{2D}\{v_z(x,y,z)\}\times H\left(k_x,k_y,(\Delta z/2)\right) \quad (8)$$

where the transfer function $H(k_x,k_y,\Delta z/2) = e^{j(\Delta z/2)\sqrt{k^2-(k_x^2+k_y^2)}}$ and Δz is the size of each propagation step. The 2D Fourier transform of normal particle velocity on the initial plane is can be obtained as (Mashouf 2009):

$$\Im_{2D}\left(v_z(x,y,z_0)\right) = w^2 \mathrm{sinc}\left(w\frac{k_x}{2\pi}, w\frac{k_y}{2\pi}\right)\times \sum_{i=1}^{N} v_i e^{-j(k_x x_{ci}+k_y y_{ci})} \quad (9)$$

where N is the total number of the array elements.
Accordingly the right hand side of Eq. (8) can be obtained by multiplying Eq. (9) to the transfer function H.
After finishing the diffraction substep**,** the result is converted back to spatial domain using inverse 2D Fourier transform and a nonlinear substep is subsequently followed as shown in Fig. 1(a). The process is then repeated to propagate the field along the z direction.

Spatial sampling

Since performing the 2D inverse Fourier transform of Eq. (8) is analytically not possible, the right hand side of this equation is discretized along k_x and k_y dimensions and an inverse discrete Fourier transform is used instead. The sampling of k_x and k_y dimensions should be performed to capture the field variations adequately. If Δx is the desired sampling interval on a propagation plane over the x dimension, the maximum spatial frequency component of the 2D discrete Fourier transform of the field over the k_x dimension is given by:

$$k_{x-\max} = \frac{\pi}{\Delta x} \quad (10)$$

As mentioned before, the first propagation step involves a diffractive sub-step which is calculated as below (see Eqs. (8) and (9)):

$$v_z\left(x,y,z_0+(\Delta z/2)\right) = \Im_{2D}^{-1}\left\{w^2 \mathrm{sinc}\left(w\frac{k_x}{2\pi}, w\frac{k_y}{2\pi}\right)\times \sum_{i=1}^{N} v_i e^{-j(k_x x_{ci}+k_y y_{ci})}\times H\left(k_x,k_y,(\Delta z/2)\right)\right\} \quad (11)$$

Studying a $\mathrm{sinc}(x)$ function shows that at around $x=5$, its amplitude has already reduced to about 5% of the maximum. Hence, the values of $w\frac{k_x}{2\pi}$ in Eq. (11) should extend beyond 5 in order for variations to be adequately captured. In other words:

$$w\frac{k_{x-\max}}{2\pi} \geq 5 \quad (12)$$

Substituting $k_{x-\max}$ form Eq. (10) into Eq. (12), the following criteria for the sampling interval is obtained:

$$\Delta x \leq w/10 \quad (13)$$

Similar criterion applies for sampling interval along y direction. In other words the spatial sampling on the propagation plane should be at least ten times finer than that of the initial plane.

Enhanced pressure formulation

In the methodology described above, the values of normal particle velocity ($\boldsymbol{v}_z$) are calculated on each propagation plane. Other acoustic parameters such as pressure should be derived from the calculated values of normal particle velocity. A simple method to convert normal particle velocity to pressure, is through the linear impedance relation as below:

$$P(x,y) = \rho_o c_o \cdot V_z(x,y) \quad (14)$$

This formula, however, is only accurate for a plane wave travelling along the z axis in an inviscid medium. As we will see later, Eq. (14) can be significantly in error in nonplanar fields. A more general formula which is valid in any field configuration (such as spherical, cylindrical or focused beams) is expressed as below (Liu and Waag 1997):

$$P(x,y)=\Im_{2D}^{-1}\left\{\Im_{2D}\{V_z(x,y)\}\frac{\rho_o c_o k}{\sqrt{k^2-(k_x^2+k_y^2)}}\right\} \quad (15)$$

Eq. (15), however, includes a singularity in spatial frequency at a circle with radius of k which is centered at origin and known as radiation circle. As a result, numerical methods to calculate the inverse Fourier transform of Eq. (15) may either fail or generate considerable amount of computational noise in the output. Eq. (15) assumes propagation in a lossless medium. In the presence of viscous loss, Eq. (15) takes the following form (see Mashouf (2009) for the full derivation):

$$P(x,y)=\Im_{2D}^{-1}\left\{\Im_{2D}\{V_z(x,y)\}\frac{\rho_o c_o \underline{k}^2}{k\sqrt{\underline{k}^2-(k_x^2+k_y^2)}}\right\} \quad (16)$$

where $\underline{k}^2=\dfrac{k^2}{1-j(2\alpha/k)}$.

In a lossless medium, $\underline{k}^2=k^2$ and Eq. (16) reduces to Eq. (15) as expected. It is interesting to note that in the presence of viscous loss, the transfer function of Eq. (16) will no longer contain a singularity. Since in a physical medium there's always some loss, the problem of singularity can therefore be avoided by using Eq. (16).

It can be also shown that in case of a plane wave propagating in an inviscid medium Eq. (16) reduces to the impedance relation of Eq. (14) as expected. In a plane wave propagating along the z direction, normal particle velocity phasor is a constant anywhere on a plane perpendicular to the z-axis. In other words $V_z(x,y)=V_o$, where V_o is a constant. As a result 2D Fourier transform of $V_z(x,y)$ is a Dirac impulse function as below:

$$\Im_{2D}\{V_z(x,y)\}=V_o\times\delta(f_x,f_y)=V_o\times\delta(\frac{k_x}{2\pi},\frac{k_y}{2\pi})=V_o\times 4\pi^2\delta(k_x,k_y) \quad (17)$$

Substituting Eq. (17) into Eq. (16) and noting that the $\delta(k_x,k_y)$ is zero everywhere except at $k_x=k_y=0$, results in:

$$P(x,y)=\Im_{2D}^{-1}\left\{V_o\times 4\pi^2\delta(k_x,k_y)\times\frac{\rho_o c_o \underline{k}^2}{k\sqrt{\underline{k}^2-(0+0)}}\right\} \quad (18)$$

or

$$P(x,y)=\Im_{2D}^{-1}\left\{V_o\times 4\pi^2\delta(k_x,k_y)\times\frac{\rho_o c_o \underline{k}}{k}\right\} \quad (19)$$

Since in an inviscid medium $\underline{k}=k$, Eq. (19) can be simplified further as below:

$$P(x,y)=\rho_o c_o \Im_{2D}^{-1}\{V_o\times 4\pi^2\delta(k_x,k_y)\} \quad (20)$$

Conversely, the inverse 2D Fourier transform of a delta function is a constant in space. In other words:

$$P(x,y)=\Im_{2D}^{-1}\{V_o\times\delta(f_x,f_y)\}=\rho_o c_o\times V_o \quad (21)$$

which is the well-known impedance relation.

Eq. (16) enables conversion of particle velocity normal to a plane to the values for pressure on the same plane. Since in our method the values of normal particle velocity are only known over the extent of propagation planes, Eq. (16) serves as an ideal tool to accomplish conversion to the values of pressure.

We refer to pressure obtained using Eq. (16) as "enhanced pressure" formulation to make distinction from the impedance pressure formulation expressed by Eq. (14). In what follows we demonstrate how impedance pressure of Eq. (14) can be significantly in error in non-planar fields.

Field of a concave spherical source

Another example of a non-planar acoustic field is the field of a concave spherical source. It is important to investigate the degree of error in the plane wave approximation used in this geometry that is frequently used in many biomedical applications including HIFU. We study three transducers with different F numbers to demonstrate how the source curvature affects the results. Focal distance of all transducers are equal (20mm) but they have different diameter of apertures as shown in Figs. 3(a). As a result, the associated F numbers of the transducers will be 2 and 1. Figs. 3(b) and (c) display the lateral pressure profiles on the focal plane of each transducer. Each graph shows two pressure profiles which have been obtained using different methods namely the Rayleigh integral and the impedance formula. The Rayleigh integral was calculated using Eq. (7), and the linear impedance formula makes use of the plane wave approximation given by Eq. (14) as described before.

As it can be seen in Fig. 3, the difference between the actual pressure and the plane wave approximation rises as the source curvature increases (or F number decreases). This is expected as deviation from a plane wave is more pronounced in the case of a highly focused source versus a slightly focused source. The second point to note about pressure profiles presented in Fig. 3, is that the actual pressure is almost always higher than what is predicted by an impedance approximation. This can be explained by the fact that in the linear impedance formula, only the normal component of particle velocity ($\boldsymbol{v}_z$) is used to estimate the pressure, but in general non-planar fields, lateral components of particle velocity (i.e. $\boldsymbol{v}_x$, $\boldsymbol{v}_y$) are also present and could have substantial amplitudes. Lateral components of the particle velocity would also contribute to creating a pressure build up.

3. Results

The KZK equation has been widely accepted as a gold-standard model to simulate nonlinear ultrasound propagation. In order to validate our methodology and test the performance of our model in nonlinear mode, we compared the results obtained using our model with published KZK simulations and experimental results. In their 1995 paper, Averkiou and Hamilton (Averkiou and Hamilton 1995) presented results of the KZK simulations for a concaved spherical source in water and compared them with experimental data. In order to do a comparative study, we implemented identical source and medium parameters (as used by Averkiou and Hamilton) in our model. The parameters used in this simulation include: Radius of

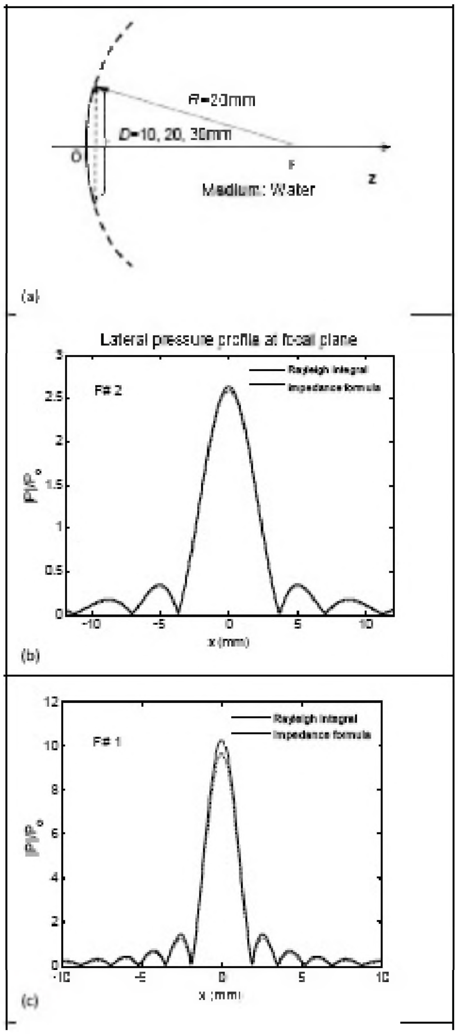

Figure 3. (a) Concentric concaved spherical sources with different diameters of aperture (*D*) to study the effect of curvature in calculation of pressure. Higher values of *D*, corresponds to higher degrees of focusing. Comparison of impedance pressure versus actual pressure at f_0 = 1 MHz on the focal plane of a (b) moderately focused and (c) a highly focused source.

curvature (R) = 160 mm, aperture diameter (D) = 37.6 mm, source pressure (P_o) = 92.5 kPa, source frequency (f_o) = 2.25 MHz, attenuation coefficient at 2.25MHz(α)= 0.1645 Np/m, and coefficient of nonlinearity (β)= 3.5.

Fig. 4 below shows the lateral pressure profiles for fundamental and three harmonics at pre-focal (z = 100 mm), focal (z = 160 mm), and post-focal (z = 250 mm) planes. The results of Averkiou and Hamilton include both experiment (solid line) and theoretical (dotted line) results. As it can be seen in Fig. 4, very good agreement exists between our results and those obtained from the KZK nonlinear model.

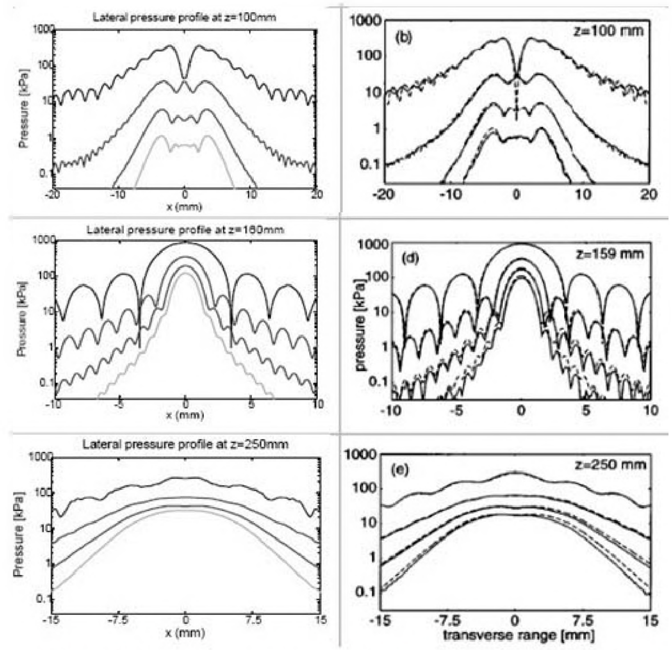

Figure 4. Lateral pressure profiles at various axial locations (top panel: pre-focal, middle panel: focal plane, bottom panel: post-focal). Left column: Our model, Right column: Experiment (solid line) and KZK results (dotted line) by Averkiou and Hamilton, 1995.

4. Discussions and Conclusions

In this work a continuous wave nonlinear propagation model based on a second-order operator splitting method was presented. The model was made more versatile by introducing a 3D arbitrary source definition capability and by converting the values of normal particle velocity to pressure across the propagation plane using an enhanced formula in dissipative media. Using our numerical model, one can define any 3D source geometry. The amplitude and phase of the normal particle velocity can also be arbitrarily defined and varied across the source surface as appropriate. This would enable simulations of transducers of arbitrary geometries and excitations. The full diffraction and enhanced pressure formula enable calculation of the acoustic pressure in a given plane in terms of the normal particle velocity in the same plane (see Eq. (16)). We demonstrated that for a concave spherical source with dimensions and excitation frequencies around those of interest in biomedical ultrasound, the impedance relation based on the plane wave approximation yields substantially lower pressure values. A particular area of interest is the focal region of focused sources where a significant difference between the two methods is observed. The difference in predicted pressure leads to even more disparity in intensity values as the intensity is related to pressure by the power of two in nonlinear regime according to the approximate formula $I_{total} \approx \sum_{n=1}^{N} I_n = \sum_{n=1}^{N} \frac{|P_n|^2}{2\rho_0 c_0}$ which simply states that the total intensity in a nonlinear field is equal to the sum of intensities of each harmonic (Bailey *et al.* 2003). Moreover, since the intensity values are directly proportional to heat generation rate, according to the approximate formula $Q_{total} \approx \sum_{n=1}^{N} 2\alpha_n I_n$ (Bailey *et al.* 2003), this will in turn affects temperature predictions as well. Accurate temperature calculations are highly demanded in areas such as ultrasound hyperthermia and/or high intensity focused ultrasound (HIFU) where focused nonlinear ultrasound beams are used to induce controlled tissue temperature elevation. Through implementation of the enhanced pressure formula we managed to resolve the singularity issue in the transfer function of normal particle velocity to pressure by making use of $\underline{k}$ or a complex wave number. By using a complex wave number, the singularity in Eq. (15) is eliminated and calculating the inverse 2D Fourier transform becomes a well-posed problem. Alternatively this singularity can be avoided by implementing a narrow band-stop filter around the singularity. However the complex wave number method offers benefits in terms of calculation accuracy and efficiency over the filtering method (Mashouf 2009).

We verified our results by comparison to simulation and experimental data available in the literature. A great agreement observed both in linear and nonlinear regimes. The next steps in this work include expansion of the current model to include temperature rise predictions, multilayer media and pulse mode propagation. The temperature simulations are carried out by calculating the heat deposition rate within the medium and coupling with an enhanced bio-heat transfer equation. Multilayer medium can be introduced into the model by changing the medium properties in each propagation step accordingly.

ACKNOWLEDGMENTS

This work was partially supported by the Ryerson Start-up Research Fund and the Natural Sciences and Engineering Research Council (NSERC) of Canada Discovery Grant that were awarded to J. Tavakkoli.

REFERENCES

Ames, W F 1992 *Numerical Methods for Partial Differential Equations* : Academic Press, New York

Averkiou, M A and Hamilton, M F 1995 Measurements of harmonic generation in a focused finite-amplitude sound beam *J. Acoust. Soc. Am.* 98 6 3439-42

Bailey, M R, Khokhlova, V A, Sapozhnikov, O A, Kargl, S G, Crum, L A, 2003 Physical mechanisms of the therapeutic effect of ultrasound (a review), *Acoustical Physics,* 49 4, 369–388

Baker, A C 1998 Nonlinear Effects in Ultrasound Propagation, *Ultrasound in Medicine* ed F A Duck, A C Baker and H C Starritt pp 23

Baker, A C, Anastasiadis, K and Humphrey, V F 1988 The nonlinear pressure field of a plane circular piston: theory and experiment *J. Acoust. Soc. Am.* 84 4 , Oct. 1988 1483-7

Baker, A C, Berg, A M, Sahin, A and Tjotta, J N 1995 The nonlinear pressure field of plane, rectangular apertures: Experimental and theoretical results *J. Acoust. Soc. Am.* 97 6 3510-7

Carstensen, E L and Bacon, D R 1998 Biomedical Applications, *Nonlinear Acoustics* ed M F Hamilton and D T Blackstock pp 421-47

Carstensen, E L, Law, W K, McKay, N D and Muir, T G 1980 Demonstration of nonlinear acoustical effects at biomedical frequencies and intensities *Ultrasound in Medicine and Biology* 6 4 359-68

Christopher, P T and Parker, K J 1991 New approaches to nonlinear diffractive field propagation *J. Acoust. Soc. Am.* 90 1 488-99

Cobbold, R S C 2007 *Foundations of Biomedical Ultrasound* : Oxford University Press

Duck, F A 2002 Nonlinear acoustics in diagnostic ultrasound *Ultrasound in Medicine and Biology* 28 1 1-18

Fay, R D 1931 Plane sound waves of finite amplitude *J. Acoust. Soc. Am.* 3 222-41

Filonenko, E A and Khokhlova, V A 2001 Effect of acoustic nonlinearity on heating of biological tissue by high-intensity focused ultrasound *Acoustical Physics* 47 4 468-75

Fubini, E 1935 Anomalie nella propagazione di onde acustiche di grande ampiezza *Alta Frequenza* 4 530-81

Hamilton, M F and Blackstock, D T ed 1998 *Nonlinear Acoustics*

Haran, M E and Cook, B D 1983 Distortion of finite amplitude ultrasound in lossy media *J. Acoust. Soc. Am.* 73 3 774-9

Kamakura, T, Ishiwata, T and Matsuda, K 2000 Model equation for strongly focused finite-amplitude sound beams *J. Acoust. Soc. Am.* 107 6 3035-46

Khokhlova, V A, Souchon, R, Tavakkoli, J, Sapozhnikov, O A and Cathignol, D 2001 Numerical modeling of finite-amplitude sound beams: Shock formation in the near field of, a cw plane piston source *J. Acoust. Soc. Am.* 110 1 95-108

Kuznetsov, V P 1971 Equations of nonlinear acoustics *Sov. Phys. Acoust.* 16 467-70

Liu, D and Waag, R C 1997 Propagation and backpropagation for ultrasonic wavefront design *IEEE Trans. Ultrason. Ferroelectr. Freq. Control* 44 1 1-13

Lucas, B G and Muir, T G 1983 Field of a finite-amplitude focusing source *J. Acoust. Soc. Am.* 74 5 1522-8

Mashouf, S 2009 An enhanced numerical model to simulate nonlinear continuous wave ultrasound propagation and the resulting temperature response *MSc. Thesis* Ryerson University, Toronto, ON, (date last viewed 5/30/2010) http://digitalcommons.ryerson.ca/dissertations/123/

Naugol'nykh, K A and Romanenko, E V 1959 Amplification factor of a focusing system as a function of sound intensity *Sov Phys Acoust* 5 191-5

Ocheltree, K B and Frizzell, L A 1989 Sound field calculation for rectangular sources. *IEEE Trans. Ultrason. Ferroelectr. Freq. Control* 36 2 242-8

Tavakkoli, J, Cathignol, D, Souchon, R and Sapozhnikov, O A 1998 Modeling of pulsed finite-amplitude focused sound beams in time domain *J. Acoust. Soc. Am.* 104 4 2061-72

Ystad, B and Berntsen, J 1996 Numerical solution of parabolic equations for strongly curved focusing sources *Acustica* 82 5 698-706

Zemp, R J, Tavakkoli, J and Cobbold, R S C 2003 Modeling of nonlinear ultrasound propagation in tissue from array transducers *J. Acoust. Soc. Am.* 113 1 139-52

Call for Papers

A Special Issue of the

International Journal of Industrial Ergonomics

OCCUPATIONNAL NOISE EXPOSURE: MEASUREMENT, ASSESSMENT AND CONTROL

Exposure to occupational noise is related to hearing loss, discomfort, fatigue and several other health and safety risks among the exposed workers. Although the research efforts over the past few decades have evolved into valuable guidelines and standards to protect workers from excessive exposures to noise, the subject of health effects, assessment and control continues to pose an array of multi-disciplinary challenges. The objective of this special issue is to compile recent research and development efforts in the field, including characterization and assessments, industrial noise control, the state of the art in the associated supporting technologies, hearing protection and perspectives on future developments and applications.

The specific topics of interest within the scope of this special issue include (but not being limited) the following:

- Characterization and assessments of workplace noise environment and noise sources;
- Hearing protection;
- Audiological and non-audiological health risks;
- Communication in noisy environments and safety issues;
- Comfort and perception issues related to workplace noise and hearing protection;
- Epidemiology;
- Standards: applications and limitations;
- Ergonomic interventions for risk control;
- Techniques for noise mitigation and industrial noise control;
- Effect of noise on human performance;
- Analytical and numerical methods for noise assessment and control.

Prospective authors are invited to submit their original works within the scope of the special issue. The authors should follow the journal guidelines (http://ees.elsevier.com/ergon/) for preparing their manuscripts, and submit electronically to either of the guest editors listed below or the journal website using the web-based submission tools. Each manuscript will be reviewed in accordance with the journal requirements.

SCHEDULE FOR SUBMISSIONS

Manuscript Submission Deadline:	3 April 2012
Reviewers' reports and decision:	26 June 2012
Final Manuscript Due on:	28 August 2012

GUEST EDITORS

R. Ramakrishnan, DSc., P.Eng
Associate Professor
Architectural Science
Ryerson University
350 Victoria Street
Toronto, Ontario, CANADA M5B 2K3
Email: rramakri@ryerson.ca

P. Marcotte, Ph.D.
IRSST
Research Department
505 boul. De Maisonneuve West
Montreal, Quebec H3A 3C2
Canada
Email: marcotte.pierre@irsst.qc.ca